Small Diameter SAG-based InGaAs/InP SPAD for 1550 nm photon counting

Ekin Kizilkan
*EPFL**
Neuchatel, Switzerland

H. K. Yildirim
EPFL
Neuchatel, Switzerland

Utku Karaca
EPFL
Neuchatel, Switzerland

Claudio Bruschini
EPFL
Neuchatel, Switzerland

Omid Salehzadeh
*NRC**
Ottawa, Canada

Anthony J. SpringThorpe
NRC
Ottawa, Canada

Alexandre W. Walker
NRC
Ottawa, Canada

Costel Flueraru
NRC
Ottawa, Canada

Oliver Pitts
NRC
Ottawa, Canada

Edoardo Charbon
EPFL
Neuchatel, Switzerland

***Abstract*—In this work, we present an InGaAs/InP-based single-photon avalanche diode (SPAD) that has a 6 µm Zn diffusion diameter. However, the device can detect photons on a circular area with a ∼21 µm diameter, even though the Zn diffusion diameter is 6 µm. We investigated potential causes of this effect together with response areas of larger diameter SPADs of the same kind. The uniform efficiency response of the 6 µm diameter device makes it a good candidate for an array implementation with a 25 µm pixel pitch.**

***Index Terms*—SPAD, InGaAs, InP, III/V, photon-counting, SWIR**

I. Introduction

InGaAs/InP single-photon avalanche diodes (SPADs) are APDs operating in Geiger mode; they are engineered for detecting photons with wavelengths up to 1700 nm, leveraging the narrow bandgap of the InGaAs absorption layer. Their high sensitivity in the shortwave infrared (SWIR) range makes them very appealing for applications in quantum information, quantum imaging, and LiDAR [1,2]. Conventionally, premature edge breakdown in these SPADs is mitigated using a double-diffused Zn layer. A selective area growth (SAG) technique with a single-step diffusion has emerged as a promising approach to reduce device noise and to achieve a more uniform response area [3]. This method involves growing an InP layer within a masked region, where the layer thickens naturally near the mask edges. A single Zn diffusion through the SAG layer results in a diffusion profile with reduced curvature at the edges, thus promoting a uniform electric field and consistent photon response across the device. However, surface nonuniformities along specific crystal orientations in the SAG layer can disrupt the Zn diffusion profile, thereby leading to anomalous sidelobes in the device's optical response [3]. Figures 1 and 2 show the cross-section and a microscope image of the device.

In this paper, we investigate the impact of a different SAG thickness on performance, particularly uniformity and noise. We have also reduced the diameter of the SAG from 70 µm, ublished in [3], down to 6, 17, and 37 µm to investigate small-diameter SPADs with a uniform response for use in large-format 2D arrays. When SAG thickness is reduced, we observed that only 6-µm diameter SPADs show a uniform response over an extended area, thus making them suitable for an array, while larger diameter devices show weaker uniformity due to insufficient SAG growth enhancement, which inadequately limits Zn diffusion along the perimeter.

*EPFL; École polytechnique fédérale de Lausanne, *NRC; National Research Council of Canada

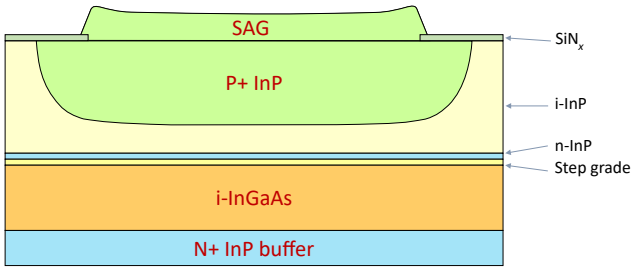

Fig. 1. Device cross-section.

Fig. 2. Microscope image of the device.

II. Measurement Results

All measurements in this work are performed in gated-mode in order to eliminate the effects of afterpulsing. The DC voltage is set one volt lower than the breakdown voltage and an AC gate voltage is superposed on it using a bias-tee

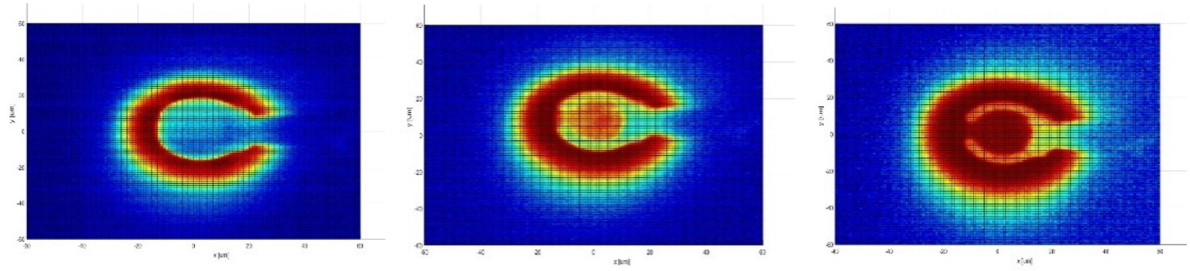

Fig. 3. Active area scans of the 37-µm device at 3, 5 and 7 V excess bias voltage.

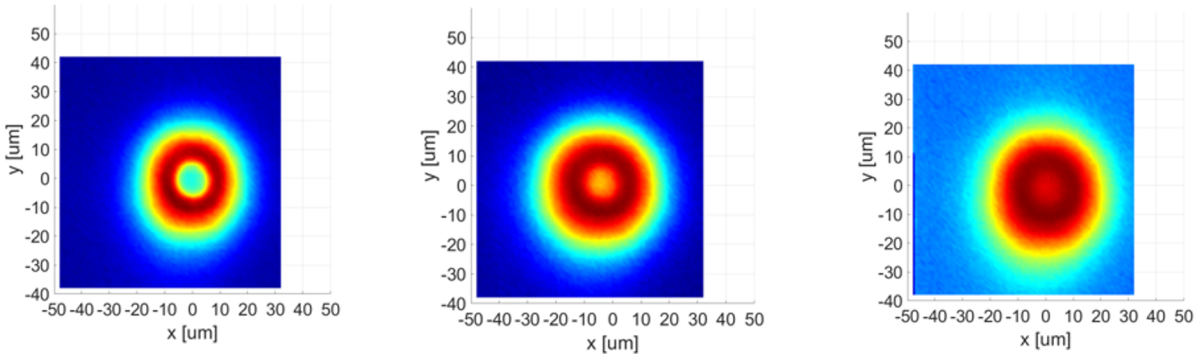

Fig. 4. Active area scans of the 17-µm device at 3, 5 and 7 V excess bias voltage.

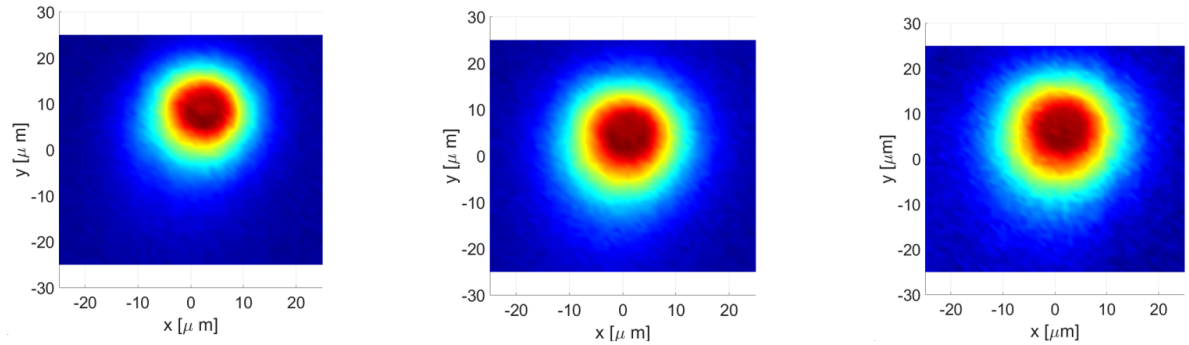

Fig. 5. Active area scans of the 6-µm device at 3, 5 and 7 V excess bias voltage.

[3]. A typical pulse duration of 50 ns is used with a 200 µs gate-off time. Figure 3 shows the active area scanning results of a SPAD with a 37-µm diameter at 3 different excess bias voltages. A confocal microscope with an objective is used to acquire these images. The 1550 nm wavelength laser beam is focused to a spot with a diameter of around 1 µm. The focused beam is moved through the SPAD surface with a step of 1 µm on a square window of 100 µm x 100 µm. At each point, the average number of counts is recorded and plotted from a top view. The red regions on the plot correspond to the regions where SPAD responds to the incoming light. The 37-µm diameter devices have a donut-shaped response at 3 V excess bias voltage. This indicates that the device suffers from edge breakdown, which is due to the enhanced electric field around the periphery. The scan results at 5 V and 7 V excess bias voltages show that the center point reaches a response level similar to that of the edge. Shadowed regions are caused by contact metal on the surface, since front-side illumination was performed for these measurements.

Figure 4 shows the scanning measurement results for a device with 17-µm active diameter. Since these devices are fully covered with the metal contact on the surface, illumination was performed through the backside. A special PCB with a hole on the back side was used for this measurement. In these scans, one can observe a donut-shaped response again at 3 V excess bias voltage with a reduced inner diameter since the active diameter of the SPAD is smaller. Finally, for the device with an active diameter of 6 µm, scan results are presented in Figure 5. For this device, a more uniform response over a diameter of 21 µm is observed thanks to a significantly

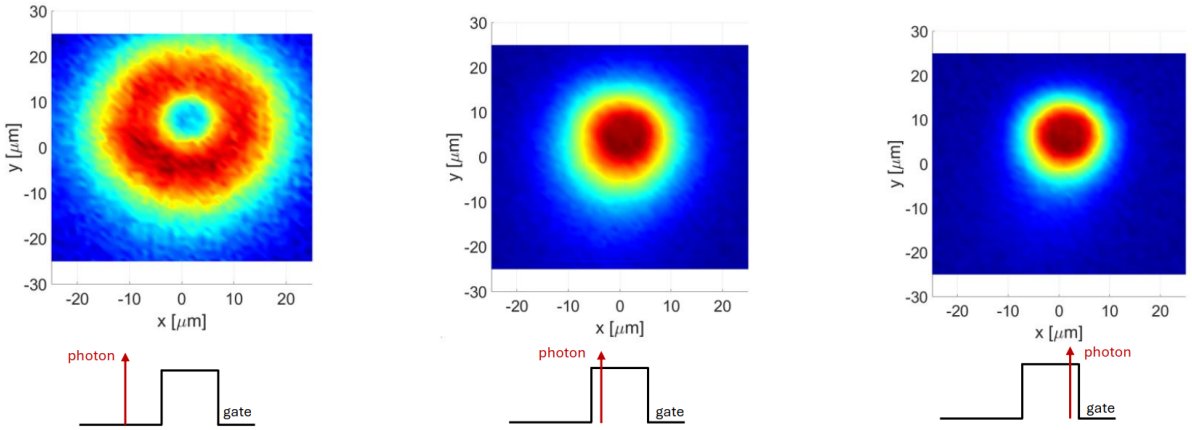

Fig. 6. Active area scans of the 6-μm device when the phase difference between the electrical gate and the laser trigger is -60 ns, 0 ns, and 40 ns, respectively.

reduced active diameter. As the inner diameter of the donut decreases, the response merges into a uniform but wider shape. The extended response diameter is caused by the curvature of the device periphery. A similar extension is also observed for the device with a 17-μm diameter. Even though large-diameter devices suffer from premature edge breakdown, causing lower efficiency at the device center, the device with a 6-μm active diameter has a flat response over a 21-μm diameter region. As a result, this device is a good candidate for an array implementation with a 25 μm pitch, with a fill factor of 84%.

Time-resolved response of the SPADs was measured using time-correlated single-photon counting (TCSPC) replacing the time-to-digital converter (TDC) with scanned time gating. A picosecond laser was used for the scan measurements of Figures 3,4, and 5. The synchronization between the electrical gate and the laser controller is adjusted such that the laser hits the device at the beginning of the electrical gate. This ensures the maximum chance of triggering an avalanche. However, it has been shown that some of the photons could still be detected even if they reach the device before turning on the electrical gate, referred to as charge persistence [4, 5]. The leftmost plot in Figure 6 demonstrates a scan result when photons impinge the device's surface 60 ns before turning on the electrical gate. In this case, the device response again forms a donut shape, but not due to premature edge breakdown. In this case, photons reach the device's surface before the junction achieves breakdown during gate-off time. Even though the electric field at the center region is not sufficient for photogenerated carriers to trigger an avalanche, it is sufficient to sweep those carriers to the anode and cathode contacts. As a result, these carriers leave the device before the gate turns on after 60 ns. On the other hand, the photocarriers that are generated around the device periphery stay longer or stay trapped at the InP/InGaAs junction [4, 5]. Consequently, those carriers have enough time until the device is turned on with the electrical gate, so they can trigger an avalanche pulse. The rightmost plot in Figure 6 shows a scan result when the photons impinge the device's surface close to the gate end. In this case, the active area is compressed and confined in a smaller diameter, as expected. Figure 7 shows the normalized count rate change when the phase difference between the laser trigger and electrical gate is swept from -160 ns to 140 ns. This data is acquired while the laser beam is located at the device center. The device turns on when the phase difference between the two is 0 ns. One can observe the steep count rate decrease when the phase difference is 50 ns, which corresponds to the gate-off instant. On the other hand, there is a strong response tail before the gate turns on. This result highlights the significance of the charge persistence effect when the efficiency is characterized under continuous illumination.

In addition to the active area scans, dark count rate (DCR) of devices with different active diameters is measured. Normalized DCR with respect to excess bias voltage are demonstrated in Figure 8. Measurements are performed at 300 K for devices with diameters of 4, 6, 7, 17, and 25 μm. The device with 7 μm diameter includes floating guard rings which is demonstrated to increase DCR [3]. Even though DCR decreases with reduced device diameter, scaling of DCR with active area is not directly proportional. Ideally, one expects a linear decrease of DCR with respect to the area due to reduced volume and reduced dark carrier generation rate. However, this proportionality would hold under the assumption that the electric field distribution within the device stays constant when the device diameter is changed. This is not the case for the devices characterized in this work. The SAG thickness depends on the mask opening which changes with the device diameter. As a result, the Zn diffusion profile and electric field distribution within the device varies. The lowest DCR per unit area is observed from the device with a 25 μm diameter (Figure 7).

Figure 9 shows the DCR change with respect to area. As discussed above, DCR decreases with a lower active area. There's a slope change in the curve for the active area smaller than 50 um^2. Since the large diameter devices in this batch suffer from edge breakdown, the electric field variation with the device diameter is more significant for that range

of devices. As a result, the DCR decrease as a function of diameter is less steep. However, as scan results indicate, the device response becomes more uniform when the device diameter is 6 µm, which could result in a more robust electric field variation when the device diameter is decreased.

Finally, Figure 10 demonstrates the DCR with respect to excess bias voltage at different temperatures for the 6-µm device; it has a DCR of 6 kcps, 29.3 kcps, 180 kcps, and 1.73 Mcps from 225 K to 300 K at 5 V excess bias, respectively.

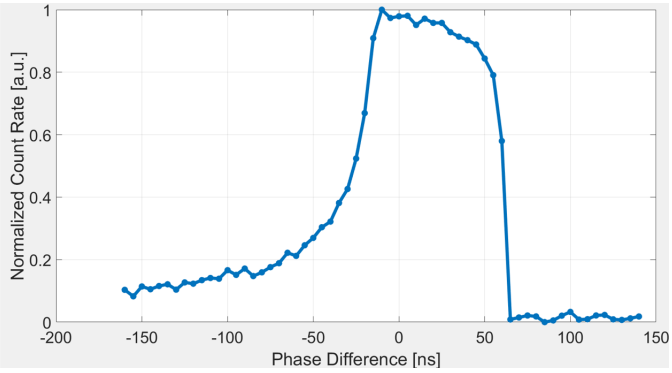

Fig. 7. Normalized count rate with respect to the phase difference between the electrical gate and the laser trigger when the laser beam is focused at the device center.

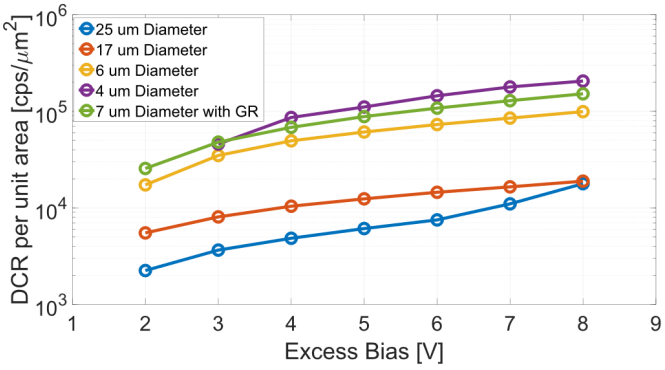

Fig. 8. Normalized DCR with respect to the excess bias for devices with different active diameters and a device with a floating guard ring.

ACKNOWLEDGMENT

This work was supported by the High-Throughput and Secure Networks Challenge Program at the National Research Council of Canada.

CONCLUSION

In this work, the response uniformity and noise performance of an InGaAs/InP-based SPAD are investigated. The Zn diffusion of the SPAD is performed by a novel method of using a SAG layer on the surface of the device. The SAG thickness varies depending on the mask opening and impacts the diffusion profile within the SPAD. Using laser scanning, a focused laser beam is directed to the SPAD, active area uniformity for different device diameters is analyzed. While

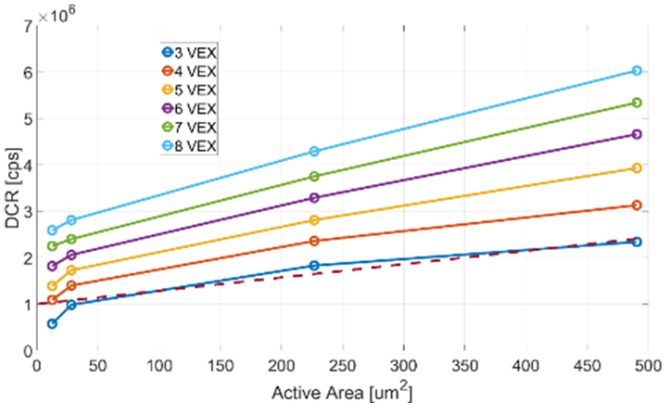

Fig. 9. DCR change with respect to active area.

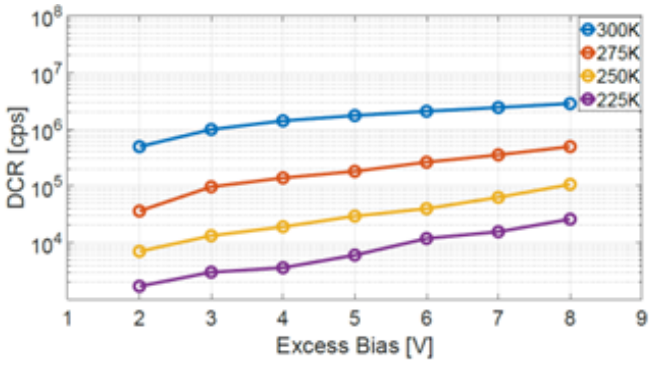

Fig. 10. DCR measurements with respect to excess bias from the 6-µm device. Measurements are performed from 225 K to 300 K.

large diameter devices demonstrate enhanced response around the device periphery, the device with 6 µm active diameter shows a relatively uniform response over an extended area. This particular SPAD is a good candidate for an SPAD array implementation of 25 µm pitch in order to reach a high fill factors in large-format imaging sensors.

REFERENCES

[1] Hadfield, Robert H. "Single-photon detectors for optical quantum information applications." Nature Photonics 3.12 (2009): 696-705.

[2] Itzler, Mark A., et al., "SWIR Geiger-mode APD detectors and cameras for 3D imaging." Advanced Photon Counting Techniques VIII. Vol. 9114. SPIE, 2014.

[3] Kizilkan, Ekin, et al., "Guard-ring-free InGaAs/InP single-photon avalanche diode based on a novel one-step Zn-diffusion technique." IEEE Journal of Selected Topics in Quantum Electronics 28.5: Lidars and Photonic Radars (2022): 1-9.

[4] Calandri, Niccolò, et al. "Charge persistence in InGaAs/InP single-photon avalanche diodes." IEEE Journal of Quantum Electronics 52.3 (2016): 1-7.

[5] Telesca, Fabio, Fabio Signorelli, and Alberto Tosi. "Double zinc diffusion optimization for charge persistence reduction in InGaAs/InP SPADs." IEEE Journal of Selected Topics in Quantum Electronics 30.1: Single-Photon Technologies and Applications (2023): 1-7.